Korean J. Chem. Eng., **26**(5), 1414-1421 (2009)
DOI: 10.2478/s11814-009-0198-3

CO_2 capture from flue gases using a fluidized bed reactor with limestone

Fan Fang, Zhen-shan Li, and Ning-sheng Cai†

Key Lab for Thermal Science and Power Engineering of the Ministry of Education (MOE),
Department of Thermal Engineering, Tsinghua University, Beijing 100084, China
(*Received 29 July 2008 • accepted 6 February 2009*)

Abstract−The CO_2 capture from flue gases by a small fluidized bed reactor was experimentally investigated with limestone. The results showed that CO_2 in flue gases could be captured by limestone with high efficiency, but the CO_2 capture capacity of limestone decayed with the increasing of carbonation/calcination cycles. From a practical point of view, coal may be required to provide the heat for $CaCO_3$ calcination, resulting in some potential effect on the sorbent capacity of CO_2 capture. Experiment results indicated that the variation in the capacity of CO_2 capture by using a limestone/coal ash mixture with a cyclic number was qualitatively similar to the variation of the capacity of CO_2 capture using limestone only. Cyclic stability of limestone only undergoing the kinetically controlled stage in the carbonation process had negligible difference with that of the limestone undergoing both the kinetically controlled stage and the product layer diffusion controlled stage. Based on the experimental data, a model for the high-velocity fluidized bed carbonator that consists of a dense bed zone and a riser zone was developed. The model predicted that high CO_2 capture efficiencies (>80%) were achievable for a range of reasonable operating conditions by the high-velocity fluidized bed carbonator in a continuous carbonation and calcination system.

Key words: CO_2 Capture, Carbonation/Calcination Reactions, Fluidized Bed Reactor, Modeling, Sorbent

INTRODUCTION

The environmental impact of anthropogenic CO_2 emissions is now recognized to be the major risk to mankind, because the CO_2 emissions into the atmosphere have been reported to account for half of the greenhouse effect which causes the global warming [1]. Therefore, reducing the CO_2 emissions will be the greatest industrial challenge of the 21st century. Recently, the process using the multiple carbonation/calcination reaction (CCR) cycles with Ca-based sorbent to capture CO_2 is considered by many researchers to be one of the suitable CO_2 separation processes from flue gases [2-4]. Fig. 1 shows a general scheme of the option. The overall system of the cyclic CCR process contains two reactors: a carbonation reactor and a calcination reactor. In the carbonator, CaO is carbonated to $CaCO_3$ at a relatively low temperature in flue gases (about 600-700 °C) at atmospheric pressure:

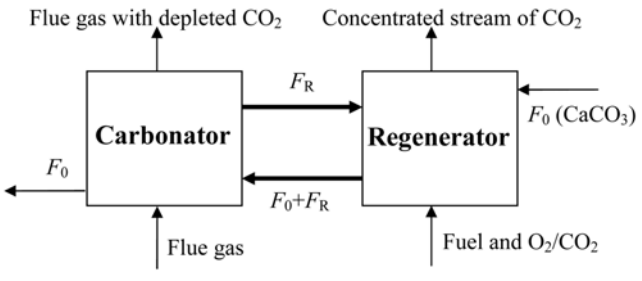

Fig. 1. Schematic of cyclic carbonation/calcination reactions using limestone to capture CO_2.

†To whom correspondence should be addressed.
E-mail: cains@tsinghua.edu.cn

$$CaO(s)+CO_2(g)\rightarrow CaCO_3(s) \quad \Delta H^0_{298}=-178\ kJ/mol \tag{1}$$

For continuous processes, the sorbent must be regenerated after the carbonation reaction to be used repeatedly. So the $CaCO_3$ is then removed from the carbonator and delivered to the regenerator. The calcination of $CaCO_3$ regenerates the sorbent to CaO and produces a concentrated stream of CO_2 at higher temperature (>900 °C):

$$CaCO_3(s)\rightarrow CaO(s)+CO_2(g) \quad \Delta H^0_{298}=178\ kJ/mol \tag{2}$$

Then the product CaO is transported to the carbonator to capture CO_2 again. In practical applications, since the reaction of CaO and CO_2 (Eq. (1)) is exothermic, steam can be produced by immersing heat transfer surfaces in the carbonator. The calcination of $CaCO_3$ (Eq. (2)) is an endothermic reaction with the heat of reaction supplied by burning fuel with pure O_2 or O_2/CO_2 in the regenerator [2].

Natural limestone, which is plentiful, cheap, and widely available, is suitable for CO_2 separation process. Many previous studies have investigated the multicycle performance of carbonation/calcination reactions of limestone and indicated that the maximum carbonation capacity decreased with the increasing number of cycles, because of the loss of a suitable pore volume and sintering between adjacent grains in the sorbent [5-9]. In practical applications, the decomposition of $CaCO_3$ is endothermic, and the required heat may be supplied by burning coal with pure oxygen diluted with CO_2 or steam in the regenerator. In the CCR process, the mineral matter in the coal ash may attach to and then react with limestone, which may affect the CO_2 capture characteristics of the sorbent. Therefore, it prompts us to examine the solid-solid interaction between the CO_2 sorbent and coal ash during multicycle carbonation/calcination reactions to examine whether the coal ash will affect the CO_2 capture capacity of the sorbent at the high temperature. Moreover, the reaction of CaO with CO_2 has two stages: kinetically controlled stage

and product layer diffusion controlled stage. Previous works [3-10] on the decay of CO_2 capture of Ca-based sorbents focused on the whole carbonation process and few previous studies considered the effect of the different carbonation stages on the sorbent performance in the CCR process. Therefore, the first objective of this study was to obtain experimental data under different conditions to examine the effect of coal ash and the different carbonation stages on the cyclic CO_2 capture and $CaCO_3$ regeneration characteristics of limestone.

The dual fluidized bed systems are widely used in various processes, such as chemical-looping combustion, sorption-enhanced steam methane reforming, chemical-looping hydrogen generation, and so on [11-14]. In the CCR process, CO_2 sorbent circulates between the carbonator and the regenerator, and the dual fluidized bed reactors being connected with solid transportation lines are considered to be a suitable system for this process [2]. For the CCR process, the main role of the regenerator is to regenerate the sorbents, and it is not necessary to deal with a large amount of gas in multiple calcination processes, so the bubbling fluidized bed reactor is considered to be appropriate as the regenerator, in which the $CaCO_3$ can be calcined more completely. Therefore, there are two types of dual fluidized bed reactors suitable for the CCR process: (1) the dual bubbling fluidized bed reactors, and (2) a bubbling fluidized bed reactor as the regenerator and a high-velocity fluidized bed reactor as the carbonator. If we use the bubbling fluidized bed reactor as the carbonator, the gas-solid contact is sufficient, and the CO_2 in flue gases is expected to be absorbed efficiently with the relatively low height of the carbonator. Fang [10] has developed a mathematical model, taking into consideration the sorbent activity loss, average carbonation rate, and mass balance between the carbonator and the regenerator, to predict the CO_2 capture in a continuous carbonation/calcination system using the dual bubbling fluidized bed reactors. However, the advantage of using the high-velocity fluidized bed reactor as the carbonator is to dispose more flue gases, and it is a better choice for a practical application. Therefore, the second purpose of this study is to develop a model to predict the CO_2 capture in a continuous carbonation/calcination system using the bubbling fluidized bed reactor as the regenerator and the high-velocity fluidized bed reactor as the carbonator to give useful information for the design of the dual fluidized bed CO_2 capture system.

EXPERIMENTAL SECTION

Multicycle tests of the carbonation and calcination reactions were carried out in a small fluidized bed reactor (0.035 m i.d.) shown in Fig. 2. The flow rates of CO_2 and N_2 from high purity cylinders controlled by mass flow controllers entered near the bottom of the reactor and were preheated before going through the distributor plate. The temperatures in the reactor measured by the thermocouple were recorded by a data acquisition system. The exit stream from the fluidized bed reactor was sampled at the outlet of the reactor

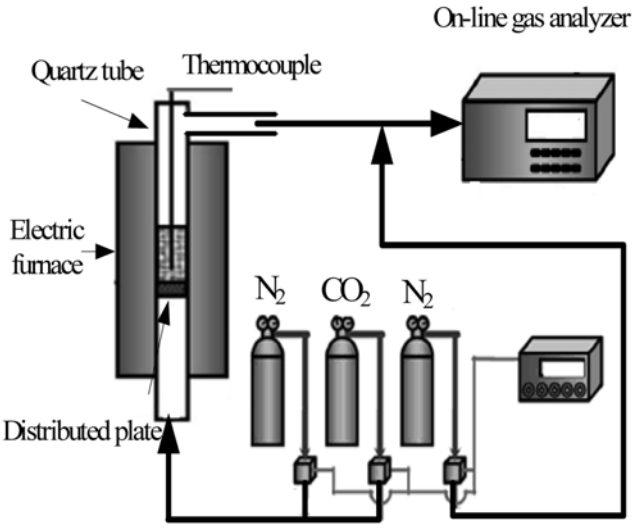

Fig. 2. Experimental bubbling fluidized bed reactor system.

and the CO_2 bulk fraction was determined by an on-line gas analyzer and recorded by a data acquisition system.

For any process using carbonation/calcination cycles, the sorbent must be regenerated in a rich CO_2 or a rich steam atmosphere in order to get high purity of CO_2 at the outlet of the regenerator. According to the thermodynamic equilibrium, $CaCO_3$ decomposition in a relatively pure CO_2 atmosphere requires a calcination temperature above 900 °C. If steam is used instead of CO_2 in the calcination stage, the calcination temperature can be reduced, but even in this case, above 850 °C will be required in order to obtain fast calcination rate. Therefore, the mild and severe calcination conditions were used in this paper. The temperature and CO_2 bulk concentration in the carbonation and calcination process can be seen in Table 1. For all the carbonation tests, the temperatures were ~650 °C, and the simulated flue gas contained 16 vol% CO_2 and the balance was nitrogen alone. For the mild calcination condition, the calcination temperature was ~850 °C, and only nitrogen flowed into the reactor. For the severe calcination condition, the calcination temperature was ~950 °C, and the gas mixture with 90 vol% CO_2 and 10 vol% N_2 flowed into the reactor.

The CO_2 fraction at the reactor outlet is always higher than 90 vol% in the calcination processes under the severe calcination condition. Because the maximum CO_2 fraction that can be measured by the gas analyzer used in this study is 50%, the calcination progress of $CaCO_3$ cannot be detected directly by the CO_2 fraction at the reactor outlet under the severe calcination condition. Therefore, in order to detect the progress of $CaCO_3$ decomposition in the fluidized bed reactor, N_2 was mixed into CO_2 stream after CO_2 stream left the outlet of fluidized bed reactor under the severe calcination condition.

Table 1. Conditions in multicycle carbonation/calcination reactions tests

	Carbonation temperature	Inlet CO_2 bulk concentration in carbonation	Calcination temperature	Inlet CO_2 bulk concentration in calcination
Mild calcination	650 °C	16%	850 °C	0%
Severe calcination	650 °C	16%	950 °C	90%

Table 2. Composition of the coal ash

	SiO_2	Al_2O_3	Fe_2O_3	K_2O	TiO_2	CaO	MgO	Others
wt%	58.098	32.396	4.596	1.446	1.334	0.994	0.365	0.771

The multicycle carbonation/calcination reactions test was as follows: when the reactor temperature was stable at 650 °C, the carbonation mixed gas (16% CO_2/84% N_2) was feed into the reactor to carry out the carbonation process. After the carbonation process, the inlet gas was switched to pure N_2 (or gas mixture with 90 vol% CO_2 and 10 vol% N_2), and the reactor temperature was adjusted to 850 °C (or 950 °C), and kept stable for some time to completely regenerate the $CaCO_3$. When the calcination process was considered to be finished, the reactor temperature was cooled to 650 °C to start the next carbonation process.

Limestone was used as the CO_2 sorbent, and it was sieved to ensure that all particles were between 200-450 μm and 90-200 μm in size. About 80-100 g sorbents were added into the reactor. The particle size of the coal ash used in the experiments was 200-450 μm, and the weight ratio of the coal ash to the limestone was 1 : 5. The composition of the coal ash is shown in Table 2.

EXPERIMENT RESULTS AND DISCUSSION

1. Effect of the Coal Ash on the CO_2 Capture Capacity of Limestone

In practical applications, since the decomposition of $CaCO_3$ is an endothermic reaction, the heat of calcination should be supplied to the regenerator. Shimizu [2] proposed that it can provide the calcination heat by burning a fraction of fuel in the regenerator with O_2/CO_2, and the coal is a suitable fuel choice. Therefore, some coal ash together with sorbents will alternate between the carbonator and the regenerator by the solid transportation lines. Kuramoto [7] found that the coal-derived ash attached to and then reacted with the Ca-based sorbents during the multiple calcination/hydration/carbonation reaction cycles in HyPr-RING process, which affected the CO_2 absorption characteristics of the sorbents. This phenomenon prompts us to examine the solid-solid interaction between the limestone and coal ash during multicycle carbonation/calcination reactions to investigate whether the interaction will affect the cyclic CO_2 capture/$CaCO_3$ regeneration characteristics and the cyclic stability of the limestone in the CCR process.

The variations of the CO_2 concentrations with the carbonation time for the 200-450 μm limestone/coal ash mixture during the CO_2 capture tests under the mild the calcination condition are shown in Fig. 3. The lime reacts with CO_2 in two stages. The initial carbonation stage is kinetically controlled with a fast reaction rate between CaO and CO_2. At this stage, the outlet CO_2 concentrations were not higher than 1% for a stable absorption period, as can been seen in Fig. 3. The experimental results of the kinetically controlled stage showed that CO_2 in the flue gases could be effectively absorbed by the limestone/coal ash mixture in the small fluidized bed reactor, which was similar to other experimental data in this study and the previous studies [9,10] using the limestone only. Fig. 3 also shows that the duration of the effective absorption period (CO_2 concentrations was not higher than 1%) decreased as the number of cycles increased because of the loss of CO_2 capture capacity of the sorbent. After the stable absorption period, CO_2 concentrations abruptly increased, indicating that the CO_2 capture capacity of the CaO was nearly exhausted. It is because a large part of active CaO was converted to $CaCO_3$ and the carbonation stage moved to the second stage controlled by the diffusion in the product layer.

After a rapid increase of the CO_2 concentration at the exit of the reactor, the CO_2 concentration increased much more slowly and trended to the inlet CO_2 level, but it could not obtain 16% even after 20 min, which meant that the sorbent still had some capacity of capturing CO_2. In the practical dual fluidized beds system, the period during which the reaction rate of CaO with CO_2 is low cannot be considered for ensuring the carbonator to be compact. After the CO_2 capture tests, the sorbents need regenerating to be used for subsequent cycles. We waited for ~20 min after the carbonation reaction reached the product layer diffusion controlled stage. Then, pure N_2 was introduced into the reactor. When the CO_2 concentration from the on-line gas analyzer was close to zero, the reactor temperature

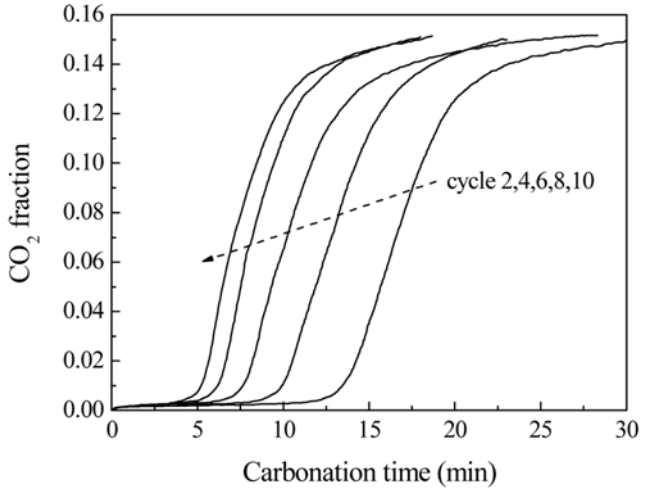

Fig. 3. CO_2 fraction with reaction time at different cycles for 200-450 μm limestone/coal ash mixture during the carbonation period under the mild calcination condition.

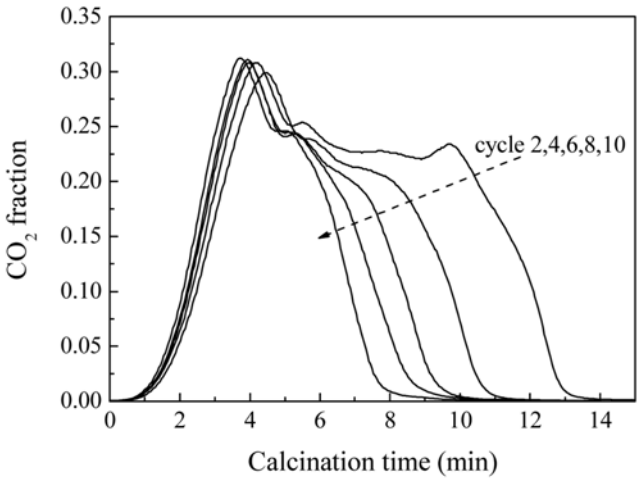

Fig. 4. CO_2 fraction with reaction time at different cycles for 200-450 μm limestone and coal ash mixture during the calcination period under the mild calcination condition.

was adjusted to 850 °C and kept stable for some time to regenerate the $CaCO_3$ completely and reactivate the sorbent. As the CO_2 concentration from the on-line gas analyzer approached zero again, the calcination process was considered finished and the reactor temperature was cooled to 650 °C again to prepare for the next carbonation process.

Fig. 4 shows the CO_2 fractions during the regeneration period as a function of time for the 200-450 μm limestone/coal ash mixture under the mild calcination period. In this study, the reactor temperature was gradually raised to 850 °C from 650 °C during the regeneration period. The heat was provided by an electric furnace with some time needed for the reactor temperature to increase from 650 °C to 850 °C. Therefore, the calcination rate was controlled by the reactor temperature. The apparent kinetic model for the conversion rate of $CaCO_3$ to CaO can be expressed as follows [15]:

$$\frac{dX_N}{dt} = k_0 \exp\left(-\frac{E}{R_g T}\right)\left(1-\frac{P_{CO_2}}{P_{e,CO_2}}\right)^n (1-X_N)^{2/3} \quad (3)$$

$$P_{e,CO_2} = 4.137\times10^7 \cdot \exp\left(-\frac{20474}{T}\right) \quad (4)$$

From Eqs. (3) and (4), it can be seen that the calcination rate of $CaCO_3$, dX_N/dt, was accelerated with the temperature increasing. Therefore, the outlet CO_2 fraction gradually increased with calcination time firstly as shown in Fig. 4. When the temperature increased greatly, the CO_2 fraction reached maximum. Then, with the increasing of regeneration time, the CO_2 fraction at the reactor exit began to decline, because the fraction of unreacted $CaCO_3$ in the reactor decreased. When all the $CaCO_3$ was calcined, no CO_2 was released from the sorbent and the CO_2 concentration approached zero at the reactor outlet. Fig. 4 also shows that the total amount of CO_2 released decreased with an increasing number of cycles because the CO_2 capture capacity of limestone decayed with the increasing of carbonation/calcination cycles.

The CO_2 capture capacity can be determined from the CO_2 concentration response curves during the carbonation processes. The carbonation conversion of the sorbent and the cyclic reactivity stability of the sorbent can be defined as:

$$X = m_{CaO}/m_{CaO}^{total} \quad (5)$$

$$Cs = \frac{X_{u,N}}{X_{u,1}} \quad (6)$$

Fig. 5 shows the sorbent cyclic stability in multiple carbonation/calcination reactions under the mild calcination condition, and indicates that with the increasing number of carbonation/calcination cycles, the cyclic stability of all the sorbent, Cs, decreased continuously. The decline of the CO_2 capture capacity with increasing number of carbonation/calcination cycles can be attributed to the changes in the structural properties of the sorbent during multiple calcinations [16]. After the reaction of CaO with CO_2, the product $CaCO_3$ must undergo calcination to regenerate CaO for repeated use. In the calcination process, some pores are produced inside the CaO particle. But at the same time, CaO sintering occurs because of the high calcination temperature, which reduces the surface area and porosity of CaO with the increasing residence time. The surface area and the porosity are very important for the reaction of CaO with CO_2, but sintering sharply reduces them, which strongly affects the CO_2 capture capacity and the carbonation reaction rates of CaO with CO_2. Therefore, with the increasing of carbonation/calcinations cyclic number, the surface area and porosity of the sorbent decreased continuously, which resulted in the decrease of the sorbent cyclic stability.

The variation in the CO_2 absorption stability of the limestone/coal ash mixture with the cyclic number was qualitatively similar to that of pure limestone of 200-450 μm and 90-200 μm, as can be seen in Fig. 5. This result clearly indicates that the particle size also had negligible effect on the cyclic reactivity, and the solid-solid interaction between the limestone and the coal ash was negligible, because they could not attach to each other well in the fluidized bed reactor.

The temperature for $CaCO_3$ decomposition in the CO_2 capture system with the carbonation/calcination cycles is critical and governed by the thermodynamics of the regeneration system. The required temperature range is from 700 °C without CO_2 in the calcination at 1 atm to 950 °C with a 100% CO_2 at 1 atm. If the process

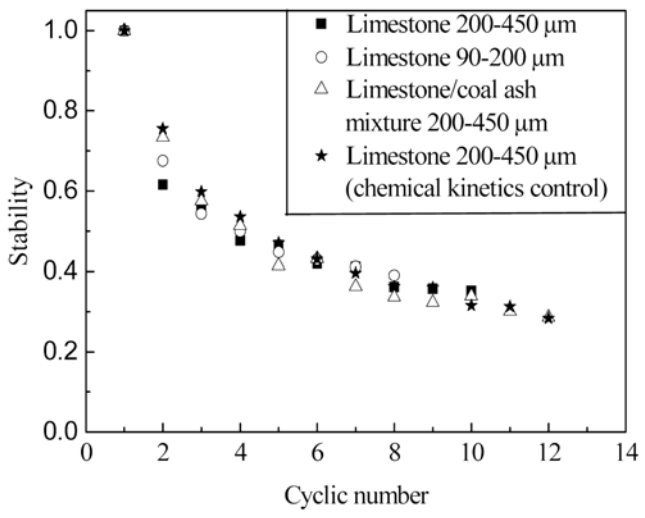

Fig. 5. Sorbent cyclic stability under the mild calcination conditions.

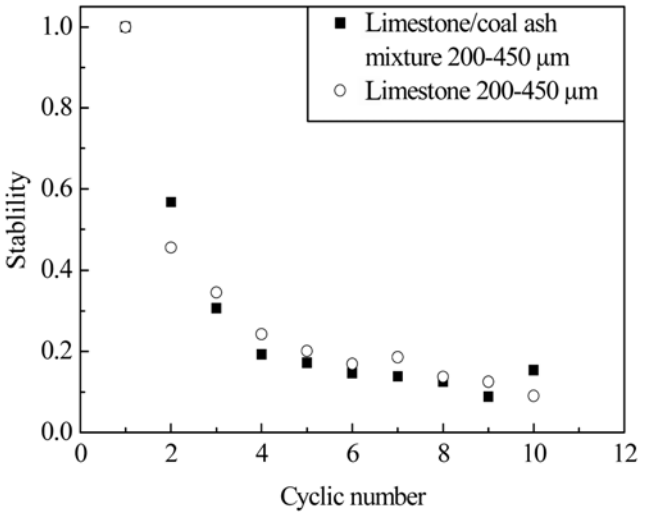

Fig. 6. Sorbent cyclic stability under the severe calcination conditions.

is operated in pursuit of as large CO_2 sequestration as possible, the regeneration of Ca-based CO_2 sorbent happens: (1) in the gas mixture with a low CO_2 fraction and a high steam fraction, and at a relatively low temperature (850 °C), or (2) in a relatively pure CO_2 stream, and a higher calcination temperature (>900 °C). Therefore, a second series of experiments with limestone and the limestone/coal ash mixture were conducted at more severe calcination conditions (950 °C calcination temperature, >90 vol% CO_2 atmosphere). Fig. 6 shows the cyclic stability under the severe calcination conditions. Under the severe calcination conditions, CO_2 absorption stabilities of both the limestone and the limestone/coal ash mixture also decreased with the cyclic number, and had identical profiles when plotted as a function of cyclic number, which meant the addition of coal ash was not a major impact on the CO_2 capture even when the temperature was very high. Comparing Fig. 5 with Fig. 6, CO_2 capture activities decreased more quickly under the severe calcination conditions than that under the mild calcination conditions. This was because the sinter during multiple calcination processes was more serious as the temperature and CO_2 concentration increased [17].

2. Effect of the Different Carbonation Stages on the CO_2 Capture Capacity of Limestone

The reaction of CaO with CO_2 has two stages. The initial stage is the kinetically controlled stage and the reaction rate of CaO with CO_2 is fast. After the fast reaction period, the product layer diffusion controlled stage happens, in which the reaction rate of CaO with CO_2 is slower. Previous works [3-10] on the decay of CO_2 capture of Ca-based sorbents focused on the whole carbonation process. The durations of the carbonation process in their experiments were longer than the kinetically controlled stage, and the CaO conversion with CO_2 was calculated by using the whole carbonation stage in their studies [3-10]. However, in practical applications, for capturing CO_2 effectively and the carbonator to be compact, only the kinetically controlled stage should be used. Therefore, the effect of the different carbonation stages on the CO_2 capture capacity of limestone was tested in this work. Fig. 7 shows the outlet CO_2 concentration and temperature in the reactor during multiple carbonation/calcination reactions under the mild calcination condition, with the sorbent only undergoing the kinetically controlled stage in the multiple carbonation reactions. At first, in the carbonation processes, the outlet CO_2 concentration was preserved not higher than 1% for a stable absorption period. After the fast absorption period, an abrupt increase in CO_2 concentration occurred. When the outlet CO_2 concentration was just higher than 4%, pure N_2 was fed into the reactor instead of 16 vol% CO_2 to make the sorbent not to experience the product layer diffusion controlled stage. Then the reactor temperature was increased to 850 °C to start the regeneration period. As can be seen from Fig. 5, the profile of the CO_2 absorption stability of limestone just undergoing kinetically controlled stage as a function of the cyclic number was not different from others. It meant that whether the sorbent undergoing the product layer diffusion controlled stage or not in the carbonation had negligible effect on the decay of CO_2 capture capacity of limestone.

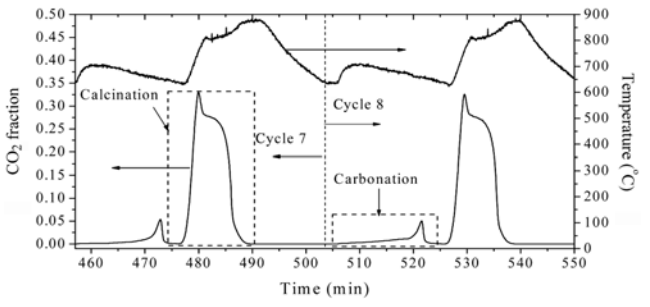

Fig. 7. CO_2 fraction and temperature with reaction time at cycle 7 and 8 for 200-450 μm limestone just undergoing kinetically controlled stage in multiple carbonation reactions.

PREDICTION OF CO_2 CAPTURE IN CONTINUOUS CARBONATION AND CALCINATION SYSTEM

1. High-velocity Fluidized Bed Carbonator Model

In practical applications, the high-velocity fluidized bed reactor is a suitable choice to be the carbonator, because it can dispose more flue gases than the bubbling fluidized bed reactor. At the same time, the bubbling fluidized bed reactor is appropriate as the regenerator, since the $CaCO_3$ can be calcined more completely in it. Therefore, it prompts us to develop a model to predict the CO_2 capture in a continuous carbonation/calcination system using the high-velocity fluidized bed reactor as the carbonator and the bubbling fluidized bed reactor as the regenerator, to give useful information for the design of the dual fluidized bed CO_2 capture system. Fig. 8 plots the schematic picture of a high-velocity fluidized bed carbonator. The carbonator has two diameters with the height change. The lower part has a larger diameter to keep low flow velocity of flue gases, which can make the gas-solid contact to be sufficient. The diameter of the upper part of the carbonator is smaller to get enough flow velocity to transport sorbents from the carbonator to the regenerator. At the same time, the variable diameter structure between the lower and upper parts makes the sorbent to get better inner circulation. Therefore, the carbonator has two different parts with the bed height as can been seen in Fig. 8: a dense bed part and a riser part. The bubbling fluidized bed model (KL model) is adapted to describe the CO_2 capture performance in the dense bed part, and the hydrodynamic model (core-annulus model) is used to predict the CO_2

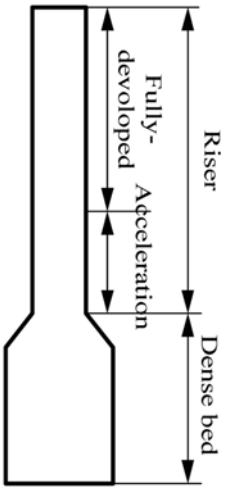

Fig. 8. Schematic of the carbonator.

capture in the riser part.

The bubbling fluidized bed model (KL model) was adopted to describe the phenomenon in the dense bed. It was assumed that there were two regions, bubble and emulsion, in a dense bed, with just one interchange coefficient, K_{be}, to represent the transfer of gas between these two regions. Based on the KL model, the CO_2 axial concentration profile in the bubble, C_{b,CO_2}, and that in the emulsion, C_{e,CO_2}, with the bed height, z, is shown as follows: [18].

$$-\delta u_b^* \frac{dC_{b,CO_2}}{dz} = \delta K_{be}(C_{b,CO_2} - C_{e,CO_2}) + \delta \gamma_b f_a K_r (C_{b,CO_2} - C_{eq,CO_2}) \quad (7)$$

$$-(1-\delta)u_{mf}\frac{dC_{e,CO_2}}{dz} = (1-\delta)(1-\varepsilon_{mf}) f_a K_r (C_{e,CO_2} - C_{eq,CO_2}) - \delta K_{be}(C_{e,CO_2} - C_{e,CO_2}) \quad (8)$$

Eq. (7) was solved with Eq. (8) simultaneously with the boundary conditions:

$$C_{b,CO_2} = C_{e,CO_2} = C_{CO_2,in} \text{ at } z=0$$

The detailed parameters and formulas required of the KL model can be found in Fang [10].

The hydrodynamic model of the riser assumed the riser to be axially composed of two zones: an acceleration zone at the riser base, where solids were accelerated to a constant upward velocity, and a fully developed flow zone extending from the end of the acceleration zone to the riser exit, where the average upward solids velocity, solid mass flux, and voidage were constant [19]. Both of the two zones postulated the existence of the core-annulus type of flow structure in the radial of the riser: dilute center region (core) and the downward flowing wall layer region (annulus).

$$u_0\left(\frac{R_c}{R}\right)^2 \frac{\partial C_{c,CO_2}}{\partial z} + \frac{2K_{ca}}{R_c}(C_{c,CO_2} - C_{a,CO_2}) + f_a K_r (1-\varepsilon_c)(C_{c,CO_2} - C_{e,CO_2}) = 0 \quad (9)$$

$$\frac{2K_{ca}R_c}{R^2 - R_c}(C_{a,CO_2} - C_{c,CO_2}) + f_a K_r (1-\varepsilon_a)(C_{a,CO_2} - C_{e,CO_2}) = 0 \quad (10)$$

Eqs. (9) and (10) described the predictive hydrodynamic model coupled with reaction kinetics, K_r, in the core and annular regions, with a mass transfer coefficient, K_{ca}, between these two regions [20]. K_{ca} equaled to 0.11 m/s by Patience [21].

The average voidage in the fully-developed flow zone is:

$$\varepsilon = \frac{u_0 \rho_s}{G_s \psi + u_0 \rho_s} \quad (11)$$

where ψ is the slip factor given by Pugsley [19]:

$$\psi = 1 + \frac{5.6}{Fr^2} + 0.47 Fr_t^{0.41} \quad (12)$$

The radius of the core region, R_c can be given by Bi [22]:

$$(R_c/R)^2 = 1.34 - 1.30(1-\varepsilon)^{0.205} + (1-\varepsilon)^{1.4} \quad (13)$$

The voidage of core region, ε_c, can be taken by a typical value as 0.995 [22]. Then, a mass balance could give the voidage of the annulus region, ε_a:

$$R^2 \varepsilon = R_c^2 \varepsilon_c + (R^2 - R_c^2)\varepsilon_a \quad (14)$$

The proposed hydrodynamic model considers the acceleration zone to be represented by the core and annulus flow structure with the assumption that the core radius in the acceleration zone equals to that evaluated for the fully developed flow zone. The model assumes that the voidage of the annulus, ε_a', in the acceleration zone varies linearly along the height of the acceleration zone from the voidage of the dense bed, ε_f, to the voidage of the annulus region, ε_a, in the fully-developed flow zone, as:

$$\varepsilon_a' = \varepsilon_f + \left(\frac{\varepsilon_a - \varepsilon_f}{L_{acc}}\right) z \quad (15)$$

The length of the acceleration zone, L_{acc}, was iteratively calculated until the particle velocity in the core region of the acceleration zone, $V_{p,c}'$, equaled to that of the fully-developed flow zone, $V_{p,c}$. The particle velocity could be calculated by a force balance on a single particle in the acceleration zone as: [19]

$$\frac{dV_{p,c}'}{dt} = \frac{3}{4} C_d \frac{\rho_g V_{sl}^2}{d_p \rho_s} + \frac{g(\rho_g - \rho_s)}{\rho_s} \quad (16)$$

$$C_d = \frac{4g(\rho_g - \rho_s)d_p}{3\rho_g (u_c/\varepsilon_c' - V_{p,c}')^2} \quad (17)$$

$$V_{p,c}' = \frac{dz}{dt} \quad (18)$$

The axial location corresponding to the time step was simply calculated from Eq. (18). The iterative procedure is shown in the flow chart of Fig. 9. First, the length of acceleration zone, L_{acc}, was guessed to determine the axial variation of the annular voidage in the acceleration zone by Eq. (15). Then L_{acc} could be iterative calculated. The detailed information could be found in Pugsley [19].

Because the bubbling fluidized bed reactor is used to be the regenerator, the $CaCO_3$ is assumed to be calcined completely in it. Therefore, at any time in the carbonator, the reactor contains three types of solids: a fraction of CaO reacting in the fast reaction regime, a fraction of inactive CaO from previous carbonation/calcination cycles, and a fraction of $CaCO_3$. f_a was defined as the fraction of active CaO in the carbonator in the continuous carbonation/calcination system:

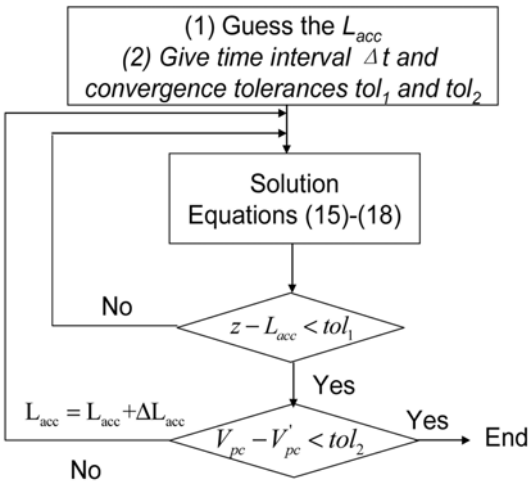

Fig. 9. Schematics of iterative procedure for solution of hydrodynamic model in the acceleration zone.

$$f_a = X_{ave} \tag{19}$$

The reaction rate constant, K_r, for the carbonation reactions was important for the prediction of the dual fluidized bed CO_2 capture system. Ca-based sorbents must undergo decay in their capacity of capturing CO_2 during multiple circulating between the carbonator and the regenerator; therefore, the makeup of fresh sorbent to the system is required as shown in Fig. 1. Corresponding to the sorbent activity loss and fresh sorbent addition, there must be sorbent undergoing 1~N cycles in the carbonator; therefore, the carbonation rate was changed with the cyclic numbers. At the same time, the sorbent undergoing the same cycle must have different residence time in the carbonator, so the carbonation rate was also different with different sorbent particles undergoing the same cycles. Fang [10] has given the average reaction rate, K_r, considered the sorbent activity loss, the mass balance, the fresh sorbent addition, and the sorbent different resident time in the carbonator:

$$K_r = \frac{\rho_{CaO}}{M_{CaO}} \cdot \sum_{N=1}^{N=\infty} \frac{F_0 F_R^{N-1}}{(F_0 + F_R)} \lambda_{ave} \tag{20}$$

where

$$a_{ave} = \frac{1}{3} k_c X_{u,N}^{-\frac{2}{3}} (\overline{C} - C_{eq,CO_2}) \tag{21}$$

$$\lambda_{ave} = k_c X_{u,N}^{-\frac{2}{3}} \left\{ X_{u,N}^{\frac{2}{3}} - \left(X_{u,N}^{\frac{1}{3}} - a_{ave}\tau \right)^2 e^{-\frac{\tau}{\tau_{ave}}} - 2a_{ave}\tau_{ave} \left[X_{u,N}^{\frac{1}{3}} - \left(X_{u,N}^{\frac{1}{3}} - a_{ave}\tau \right) e^{\frac{\tau}{\tau_{ave}}} \right] + 2(a_{ave}\tau_{ave})^2 \left(1 - e^{\frac{\tau}{\tau_{ave}}} \right) \right\} \tag{22}$$

and k_c=0.0021 $m^3/(mol \cdot s)$ for the kinetically controlled stage.

2. Prediction of CO_2 Capture in the High-velocity Fluidized-bed Carbonator

Incorporating Eq. (20) into the KL and hydrodynamic models, the simulated results of CO_2 capture in the continuous carbonation/calcination system could be obtained. The standard inputs of a lab-scale carbonation reactor used here are presented in Table 3. Limestone was used as the CO_2 sorbent, and regenerated under the severe calcination conditions (950 °C and >90 vol% CO_2 atmosphere) in the regenerator.

The profile of the average CO_2 concentration with carbonator height is shown as Fig. 10. If the exit CO_2 concentration is below 3%, about 83% CO_2 in the flue gas is absorbed by the sorbent in the carbonator. From Fig. 10, if the average conversion, X_{ave}, was 0.08, ~74.3% of the CO_2 in the flue gas was captured by the dense bed part, and finally ~83.8% CO_2 was captured at the exit of the riser. The addition of more fresh sorbent into the system gave an

Table 3. Parameter of prediction of CO_2 capture by a lab-scale carbonation reactor

d_{dense}	d_{riser}	d_p	H_{dense}
0.1 m	0.04 m	350 μm	1 m
H_{riser}	Inlet flue gas	Vol% CO_2	ρ_s
4 m	14.13 m^3/h	15	1,580 kg/m^3

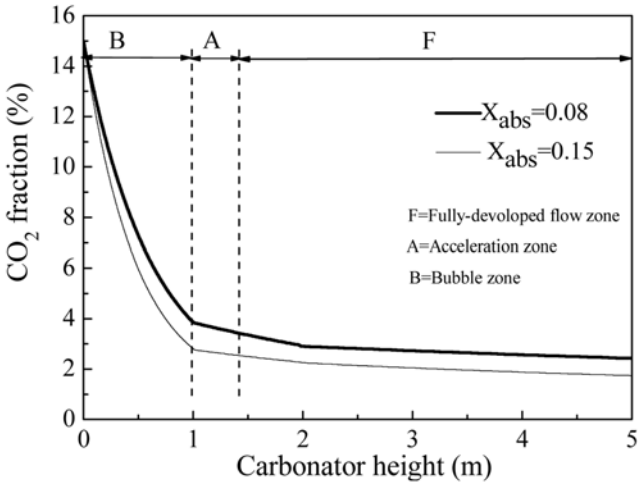

Fig. 10. Predictive CO_2 fraction with bed height of carbonator in a continuous carbonation and calcination system.

average CaO conversion, X_{ave}, of 0.15, and ~81.3% CO_2 was captured by the dense bed part, and ~88.4% of the CO_2 was captured at the exit of riser. It meant that with the increasing of CaO average conversion, X_{ave}, the efficiency of CO_2 removal was improved. At the same time, the lowest solid circulation rate between the carbonator and the regenerator, which must be high enough to transfer the regenerated sorbents necessary for the CO_2 capture, is between 2.33-4.16 $kg/(m^2 \cdot s)$. With increasing X_{ave}, the solid circulation rate between the carbonator and the regenerator decreased, and it would decrease the cost of operation. However, the amount of fresh sorbent (F_0) for X_{ave}=0.15 was 2.81 times as much as that for X_{ave}= 0.08, which would increase the cost of the sorbents. Conclusively, the total cost of CCR process increased as X_{ave} increased [4].

From Fig. 10, the CO_2 in the flue gas was mainly captured by the dense bed region of the carbonator, because the gas-solid contact was sufficient for the larger amount of sorbents and low gas flow velocity in the dense bed region. When the flue gas flowed into the acceleration zone, the diameter of the carbonator became smaller, causing the higher gas velocity and higher void fraction. Therefore, the CO_2 was not efficiently captured in the acceleration zone. In the fully developed flow zone, the CO_2 capture became worse for the highest void fraction in the carbonator.

CONCLUSIONS

The cyclic CO_2 capture and $CaCO_3$ regeneration characteristics in a small fluidized bed reactor were experimentally investigated with limestone. A model (KL model and hydrodynamic model), combining the mass balance and average carbonation rate, was developed to predict the CO_2 capture in a continuous carbonation/calcination system using a lab-scale high-velocity fluidized bed carbonator and a bubbling fluidized bed regenerator. The main conclusions were the following:

(1) CO_2 could be captured by limestone with high efficiency, but the CO_2 capture capacity of limestone decayed with the increasing of carbonation/calcination cycles, especially under the severe calcination conditions;

(2) The coal ash, different carbonation reaction stage, and parti-

cle size had negligible effect on the capacity decay of CO_2 capture of limestone with the cyclic number;

(3) The model predicted that high CO_2 capture efficiencies (>80%) were achievable for a range of reasonable operating conditions by a lab-scale high-velocity fluidized bed carbonator in a continuous carbonation/calcination system. The CO_2 in the flue gas was mainly captured by the dense bed part of the carbonator and the efficiency of CO_2 removal was improved by the increasing of CaO average conversion.

ACKNOWLEDGMENTS

This work was supported by the National Basic Research Program of China (2006CB705807) and the National Natural Science Funds of China (No. 50806038).

NOMENCLATURE

$\overline{C}$: average concentration of reacting gas [mol m^{-3}]
C_{CO_2} : concentration of CO_2 [mol m^{-3}]
$C_{CO_2,in}$: total CO_2 concentration at the reactor entrance [mol m^{-3}]
C_{eq,CO_2}: equilibrium concentration of CO_2 over CaO [mol m^{-3}]
C_d : drag coefficient
d : diameter [m]
F_0 : molar flow rate of added fresh sorbents [kmol s^{-1}]
F_R : sorbent molar flow rates from the carbonator to the regenerator [kmol s^{-1}]
Fr : Froude number
f_a : fraction of active CaO in the carbonation process
G_s : net solids mass flux [kg m^{-2} s^{-1}]
g : 9.8 m s^{-2}, acceleration of gravity
H : height [m]
K_{ca} : coefficient of gas interchange between the core and annular regions [m s^{-1}]
K_{be} : coefficient of gas interchange between bubble and emulsion phase [s^{-1}]
K_r : chemical rate constant [s^{-1}]
k_c : chemical rate constant in the carbonation process [m^3 mol^{-1} s^{-1}]
k_0 : effective reaction rate constant in the calcination process [s^{-1}]
m_{CaO} : CaO mass reacting with CO_2 [kg]
m_{CaO}^{total} : total mass of CaO in sorbents [kg]
M_{CaO} : molecular weight of CaO [kg mol^{-1}]
P : pressure [Pa]
P_{e,CO_2} : equilibrium pressure of CO_2 over CaO [Pa]
R : radius [m]
T : temperature [K]
t : time [s]
V_p : solids velocity [m s^{-1}]
V_{sl} : slip velocity [m s^{-1}] $(=(u_{g,c}/\varepsilon_c)-V_p)$
$u_{g,c}$: gas velocity in the core region [m s^{-1}] $(=u_0/(R_c/R)^2)$
u_0 : superficial gas velocity [m s^{-1}]
u_{mf} : superficial gas velocity at the minimum fluidizing conditions [m s^{-1}]
u_b^* : rise velocity of bubble gas [m s^{-1}]
X_{ave} : CaO average conversion
X_N : carbonation conversion at the Nth cycle
$X_{u,X}$: final carbonation conversion at the Nth cycle
z : height [m]

Greek Letters

γ_b : volume of solids dispersed in bubbles
δ : bubble fraction in the bed
ε : void fraction
ε_{mf} : void fraction in the bed at the minimum fluidized conditions
ε_f : void fraction in the dense bed
ρ : density [kg m^{-3}]
τ_{ave} : average solid residence time in carbonation [s]
ψ : slip factor

Subscripts

acc : acceleration region
a : annulus phase
b : bubble phase
c : core phase
dense : dense bed part
riser : riser part
e : emulsion phase
g : gas phase
s : solid phase

REFERENCES

1. J. T. Houghton, *Climate change 1995: The science of climate change*, Cambridge University Press Publications, Cambridge (1996).
2. T. Shimizu, T. Hirama, H. Hosoda, K. Kitano, M. Inagaki and K. Tejima, *Trans. IChemE.*, **77**, 62 (1999).
3. J. C. Abanades, E. J. Anthony, D. Y. Lu, C. Salvador and D. Alvarez, *AIChE J.*, **50**, 1614 (2004).
4. Z. S. Li, N. S. Cai and C. Eric, *AIChE J.*, **54**, 1912 (2008).
5. Z. S. Li, N. S Cai and Y. Y. Huang, *Ind. Eng. Chem. Res.*, **45**, 1911 (2006).
6. Z. S. Li, N. S. Cai, Y. Y. Huang and H. J. Han, *Energy & Fuels*, **19**, 1447 (2005).
7. K. Kuramoto, S. Shibano, S. Fujimoto, T. Kimura, Y. Suzuki, H. Hatano, S. Y. Lin, M. Harada, K. Morishita and T. Takarada, *Ind. Eng. Chem. Res.*, **42**, 3566 (2003).
8. J. C. Abanades and D. Alvarez, *Energy & Fuels*, **17**, 308 (2003).
9. H. J. Ryu, J. R. Grace and C. J. Lim, *Energy & Fuels*, **20**, 1621 (2006).
10. F. Fang, Z. S. Li and N. S. Cai, *Energy & Fuels*, **23**, 207 (2009).
11. H. J. Ryu, Y. C. Park, S. H. Jo and M. H. Park, *Korean J. Chem. Eng.*, **25**, 1178 (2008).
12. G. T. Jin, H. J. Ryu, S. H. Jo, S. Y. Lee, S. R. Son and S. D. Kim, *Korean J. Chem. Eng.*, **24**, 542 (2007).
13. K. S. Song, Y. S. Seo, H. K. Yoon and S. J. Cho, *Korean J. Chem. Eng.*, **20**, 471 (2003).
14. H. J. Ryu and G. T. Jin, *Korean J. Chem. Eng.*, **24**, 527 (2007).
15. Z. S. Li, F. Fang and N. S. Cai, *Journal of Engineering for Thermal Energy and Power*, **22**, 642 (2007).
16. A. Silaban and P. Harrison, *Chem. Eng. Commun.*, **137**, 177 (1995).
17. R. H. Borgwardt, *Ind. Eng. Chem. Res.*, **28**, 493 (1989).
18. D. Kunii and O. Levenspiel, *Ind. Eng. Chem. Res.*, **29**, 1226 (1990).
19. T. S. Pugsley and F. Berruti, *Powder Technology*, **89**, 57 (1996).
20. T. S. Pugsley and F. Berruti, *Chem. Eng. Sci.*, **51**, 2751 (1996).
21. G. S. Patience and J. Chaouki, *Chem. Eng. Sci.*, **48**, 3195 (1993).
22. H. T. Bi, *Can. Jour. Chem. Eng.*, **80**, 809 (2002).